A Single Dose of ^{225}Ac-RPS-074 Induces a Complete Tumor Response in an LNCaP Xenograft Model

James M. Kelly[1,2], Alejandro Amor-Coarasa[1,2], Shashikanth Ponnala[1,2], Anastasia Nikolopoulou[1,3], Clarence Williams, Jr.[1,2], Nikki A. Thiele[4], David Schlyer[5], Justin J. Wilson[4], Stephen G. DiMagno[6], and John W. Babich[1–3,7]

[1]Division of Radiopharmaceutical Science, Department of Radiology, Weill Cornell Medicine, New York, New York; [2]Molecular Imaging Innovations Institute (MI3), Department of Radiology, Weill Cornell Medicine, New York, New York; [3]Citigroup Biomedical Imaging Center, Weill Cornell Medicine, New York, New York; [4]Department of Chemistry and Chemical Biology, Cornell University, Ithaca, New York; [5]Brookhaven National Laboratory, Upton, New York; [6]College of Pharmacy, University of Illinois–Chicago, Chicago, Illinois; and [7]Sandra and Edward Meyer Cancer Center, Weill Cornell Medicine, New York, New York

Promising biochemical responses to ^{225}Ac-prostate-specific membrane antigen (PSMA) 617, even in patients who are refractory to β-particle radiation, illustrate the potential of targeted α-therapy for the treatment of metastatic castration-resistant prostate cancer. However, side effects such as xerostomia are severe and irreversible. To fully harness the potential of targeted α-therapy, it is necessary to increase the therapeutic index of the targeted radioligands. One emerging strategy is to increase clearance half-life through enhanced binding to serum albumin. We have evaluated the albumin-binding PSMA-targeting ligand RPS-074 in a LNCaP xenograft model to determine its potential value to the treatment of prostate cancer. **Methods:** ^{225}Ac-RPS-074 was evaluated in male BALB/c mice bearing LNCaP xenograft tumors. A biodistribution study was performed over 21 d to determine the dosimetry in tumors and normal tissue. The dose response was measured in groups of 7 mice using 37, 74, and 148 kBq of ^{225}Ac-RPS-074 and compared with positive and negative control groups. Mice were sacrificed when tumor volume exceeded 1,500 mm^3. **Results:** ^{225}Ac-RPS-074 was labeled in greater than 98% radiochemical yield and showed high (>10% injected dose/g) and sustained accumulation in LNCaP tumors from 24 h to beyond 14 d. Signal in blood and highly vascularized tissues was evident over the first 24 h after injection and cleared by 7 d. The tumor-to-kidney ratio was 4.3 ± 0.7 at 24 h and 62.2 ± 9.5 at 14 d. A single injection of 148 kBq induced a complete response in 6 of 7 tumors, with no apparent toxic effects. Treatment with 74 kBq induced a partial response in 7 of 7 tumors, but from 42 d, 6 of 7 experienced significant regrowth. The 37-kBq group experienced a survival benefit relative to the negative control but not compared with the positive control group. **Conclusion:** A single dose of 148 kBq of ^{225}Ac-RPS-074 induced a complete response in 86% of tumors, with tumor–to–normal-tissue ratios that predict an improved therapeutic index. The use of the macropa chelator enabled quantitative radiolabeling and may facilitate the clinical translation of this promising targeted α-therapeutic.

Key Words: targeted alpha therapy; ^{225}Ac; PSMA; complete tumor response

J Nucl Med 2019; 60:649–655
DOI: 10.2967/jnumed.118.219592

The treatment of late-stage, metastatic castration-resistant prostate cancer by targeted radioligand therapy is rapidly emerging as a promising option for extension of life, with acceptable side effects (*1*). Ligands labeled with the β-emitting ^{177}Lu, such as ^{177}Lu-prostate-specific membrane antigen (PSMA) 617 (*2–6*) and ^{177}Lu-PSMA-I&T (*7–8*), have been shown to induce at least a 50% decrease in PSA in 30%–60% of patients after a single cycle or multiple cycles of therapy, with only mild-to-moderate, reversible side effects evident even after multiple therapy cycles. Other ligands labeled with the β-emitting ^{131}I, such as ^{131}I-MIP-1095, have induced even more dramatic responses, though the reported side effects were more severe (*9–10*).

Despite these encouraging reports, more than 30% of patients never respond to β-particle radioligand therapy, the relapse rate remains high, and the response after multiple therapy cycles often decreases (*11*). The limitations of current therapies may be linked to insufficient dose delivery to the tumor (*12*), with this insufficient delivery being a product of suboptimal pharmacokinetics of the delivery vector and the low linear-energy transfer intrinsic to β-particles. When patients with metastatic castration-resistant prostate cancer were treated with the α-emitting ^{225}Ac-PSMA-617, full biochemical responses were observed in some patients, even in those who had not responded to treatment with ^{177}Lu-PSMA-617 (*11*). However, severe and irreversible xerostomia significantly limits the potential utility of this promising approach (*13*).

To enable the therapeutic potential of ^{225}Ac, which has a half-life (10.0 d) that permits rapid initial uptake and clearance from normal tissue but requires sustained tumor uptake and retention, and induces DNA double-strand breaks by emission of 4 α-particles with high linear-energy transfer, we aimed to design a high-affinity, low-molecular-weight ligand for the PSMA-targeted radioligand therapy that stably chelates $^{225}Ac^{3+}$ and uses albumin binding to modulate blood clearance, tumor uptake and uptake kinetics, and reduces access to nontarget tissue. We report herein the synthesis and in vitro characterization of RPS-074 and its

Received Aug. 28, 2018; revision accepted Oct. 3, 2018.
For correspondence or reprints contact: John W. Babich, Department of Radiology, Weill Cornell Medicine, Belfer Research Building, Room 1600, 413 E. 69th St., New York, NY 10021.
E-mail: job2060@med.cornell.edu
Published online Nov. 9, 2018.

evaluation as a potential radiotherapeutic in a preclinical model of human prostate cancer.

MATERIALS AND METHODS

Chemistry

The synthesis of (((*S*)-1-carboxy-5-(3-(3-(1-((14*S*,45*S*)-45-carboxy-14-(4-(3-(2-carboxy-6-((16-((6-carboxypyridin-2-yl)methyl)-1,4,10,13-tetraoxa-7,16-diazacyclooctadecan-7-yl)methyl)pyridin-4-yl)thioureido)butyl)-54-(4-iodophenyl)-12,15,43,51-tetraoxo-3,6,9,19,22,25,28,31,34,37,40-undecaoxa-13,16,44,50-tetraazatetrapentacontyl)-1H-1,2,3-triazol-4-yl)phenyl)ureido)pentyl)carbamoyl)-L-glutamic acid (RPS-074) is described in full in the Supplemental Data (Supplemental Fig. 1; supplemental materials are available at http://jnm.snmjournals.org). Briefly, RPS-074 was generated from the coupling of di-*tert*-butyl (((*S*)-1-(*tert*-butoxy)-6-(3-(3-ethynylphenyl)ureido)-1-oxohexan-2-yl)carbamoyl)-L-glutamate (*14*), macropa-isothiocyanate (*15*), and N^6-(4-(4-iodophenyl)butanoyl)-L-lysine by 2 linkers with 3 and 8 PEG units, respectively. RPS-072 was synthesized following a previously published method (*16*).

Radiochemistry

All reagents were purchased from Sigma Aldrich unless otherwise noted and were of reagent grade. HCl was traceSELECT (>99.999%; Honeywell Research Chemicals) for trace analysis quality. Aluminum-backed silica thin-layer chromatography (TLC) plates were purchased from Sigma Aldrich. Stock solutions of 0.05 M HCl and 1 M NH_4OAc were prepared by dilution in Milli-Q water (MilliporeSigma).

^{225}Ac-RPS-074. To a solution of $^{225}Ac(NO_3)_3$ (Oak Ridge National Laboratory) in 0.05 M HCl (16.7–21.0 MBq in 950 μL) were added 20 μL of a 1 mg/mL solution of RPS-074 in dimethyl sulfoxide. The pH was increased to 5–5.5 by addition of 90 μL of 1 M NH_4OAc. The reaction was gently shaken for 20 min at 25°C on an Eppendorf Thermomixer C (VWR). Then, the reaction was diluted with H_2O (9 mL) and passed through a preactivated Sep-Pak C18 Light cartridge (Waters). The reaction vial and cartridge were washed with H_2O (5 mL), and the product was eluted with 500 μL of EtOH followed by 500 μL of normal saline (0.9% NaCl in deionized H_2O; VWR). The eluate was diluted to 4 mL in normal saline to give a stock solution with a radioactivity concentration of 1.1–1.5 MBq/mL.

An aliquot was removed from the final solution and spotted onto an aluminum-backed silica TLC plate to determine radiochemical impurity. An aliquot of the $^{225}Ac(NO_3)_3$ solution in 0.05 M HCl was spotted in a parallel lane as a control. The plate was immediately run in a 10% v/v MeOH/10 mM ethylenediaminetetraacetic acid mobile phase and then allowed to stand for 8 h to enable radiochemical equilibrium to be reached. The plate was visualized on a Cyclone Plus Storage Phosphor System (Perkin Elmer) after a 2-min exposure on the phosphor screen. The radiochemical purity was expressed as a ratio of ^{225}Ac-RPS-074 to total activity and was determined to be 98.1%. The plate was visualized again 16 h later to confirm purity.

^{225}Ac-RPS-072. To a solution of $^{225}Ac(NO_3)_3$ in 0.05 M HCl (7.7 MBq in 950 μL) were added 20 μL of a 1 mg/mL solution of RPS-072 in dimethyl sulfoxide. The pH was increased to 5–5.5 by addition of 105 μL of NH_4OAc, and the reaction was heated for 20 min at 95°C on an Eppendorf Thermomixer C. Then, the reaction mixture was diluted with H_2O (9 mL) and passed through a preactivated Sep-Pak C18 Light cartridge. The reaction vial and cartridge were washed with H_2O (5 mL), and the product was eluted with 100 μL of EtOH followed by 900 μL of normal saline (0.9% NaCl in deionized H_2O). The final product mixture was further diluted with 1 mL of saline to give a stock solution with a radioactivity concentration of 1.05 MBq/mL. Radiochemical purity was determined by radio-TLC according to the procedure described above.

^{225}Ac-DOTA-Lys-4-(4-iodophenyl)butanoic Acid (IPBA). To a solution of $^{225}Ac(NO_3)_3$ in 0.05 M HCl (5.0 MBq in 900 μL) were added 30 μL of a 1 mg/mL solution of DOTA-Lys-IPBA in dimethyl sulfoxide. The pH was increased to 5 by addition of 50 μL of 1 M NH_4OAc, and the reaction was heated for 25 min at 95°C on an Eppendorf Thermomixer C. Then, the reaction mixture was diluted with H_2O (9 mL) and passed through a preactivated Sep-Pak C18 Light cartridge. The reaction vial and cartridge were washed with H_2O (5 mL), and the product was eluted with 200 μL of a 50% v/v EtOH/saline solution followed by 800 μL of normal saline (0.9% NaCl in deionized H_2O). Radiochemical purity was determined by radio-TLC as described above.

Cell Culture

The PSMA-expressing human prostate cancer cell line, LNCaP, was obtained from the American Type Culture Collection. Cell culture supplies were obtained from Invitrogen unless otherwise noted. LNCaP cells were maintained in RPMI-1640 medium supplemented with 10% fetal bovine serum (Hyclone), 4 mM L-glutamine, 1 mM sodium pyruvate, 10 mM *N*-2-hydroxyethylpiperazine-*N*-2-ethanesulfonic acid, a 2.5 mg/mL solution on D-glucose, and a 50 μg/mL solution on gentamicin in a humidified incubator at 37°C and 5% CO_2. Cells were removed from flasks for passage or for transfer to 12-well assay plates by incubating them with 0.25% trypsin and ethylenediaminetetraacetic acid.

In Vitro Determination of Half-Maximal Inhibitory Constant (IC_{50})

The IC_{50} value of the nonlabeled, metal-free RPS-074 was determined by screening in a multiconcentration competitive binding assay against ^{99m}Tc-((7*S*,12*S*,16*S*)-1-(1-(carboxymethyl)-1*H*-imidazol-2-yl)-2-((1-(carboxymethyl)-1*H*-imidazol-2-yl)methyl)-9,14-dioxo-2,8,13,15-tetraazaoctadecane-7,12,16,18-tetracarboxylic acid technetium tricarbonyl complex (^{99m}Tc-MIP-1427), with a dissociation constant of 0.64 ± 0.46 nM (*17*) for binding to PSMA on LNCaP cells, according to previously described methods (*18*) with small modifications. Briefly, LNCaP cells were plated 72 h before the experiment to achieve a density of approximately 5×10^5 cells per well (in triplicate) in RPMI-1640 medium supplemented with 0.25% bovine serum albumin. The cells were incubated for 2 h with 1 nM ^{99m}Tc-MIP-1427 in RPMI-1640 medium containing 0.00125% w/v bovine serum albumin (*19*) in the presence of 0.001–10,000 nM test compounds. Radioactive incubation medium was then removed by pipette, and the cells were washed twice using 1 mL of ice-cold phosphate-buffered saline ×1 solution. Cells were harvested from the plates after treatment with 1 mL of 1 M NaOH and transferred to tubes for radioactive counting using a 2470 Wizard^2 automatic γ-counter (Perkin Elmer). Standard solutions (10% of activity added to each well) were prepared to enable decay correction. Cell-specific activity was corrected for nonspecific binding of ^{99m}Tc-MIP-1427. IC_{50} values were determined by fitting the data points to a sigmoidal Hills1 curve in Origin software (OriginLab).

Inoculation of Mice with Xenografts

All animal studies were approved by the Institutional Animal Care and Use Committee of Weill Cornell Medicine and were undertaken in accordance with the guidelines set forth by the U.S. Public Health Service policy on humane care and use of laboratory animals. Animals were housed under standard conditions in approved facilities with 12-h light–dark cycles. Food and water were provided ad libitum throughout the course of the studies. Male BALB/c athymic *nu/nu* mice were purchased from the Jackson Laboratory. For inoculation in mice, LNCaP cells were suspended at 4×10^7 cells/mL in a 1:1 mixture of phosphate-buffered saline:Matrigel (BD Biosciences). Each mouse was injected in the left flank with 0.25 mL of the cell suspension. Biodistributions were conducted when tumors were in the range of 200–800 mm^3, and therapy studies were initiated when tumors were in the range of 50–900 mm^3.

Biodistribution Studies in LNCaP Xenograft Mice

LNCaP xenograft tumor-bearing mice (4 per time point per compound) were injected intravenously with a bolus injection of 105 kBq and 320 ng (142 pmol) of ^{225}Ac-RPS-074. The mice were sacrificed at 4 h, 24 h, 7 d, 14 d, and 21 d after injection. A blood sample was removed, and a full biodistribution study was conducted on the following organs (with contents): heart, lungs, liver, small intestine, large intestine, stomach, spleen, pancreas, kidneys, muscle, bone, and tumor. Tissues were weighed and counted on a 2470 Wizard^2 automatic γ-counter. Standards of 1% injected dose were prepared to enable quantification of tissue uptake. Counts were corrected for decay and for activity injected, and tissue uptake was expressed as percentage injected dose per gram (%ID/g). SE measurement was calculated for each data point.

LNCaP xenograft tumor-bearing mice ($n = 4$) were injected intravenously with a bolus injection of 105 kBq and 900 ng (407 pmol) of ^{225}Ac-RPS-072 and were sacrificed at 24 h after injection. The biodistribution study was performed as described above.

Therapy Study in LNCaP Xenograft Mice

LNCaP xenograft tumor-bearing mice were randomly assigned to 5 groups (7 mice per group). One group was injected intravenously with a bolus injection of 148 kBq and 93 ng (41 pmol) of ^{225}Ac-RPS-074. The second treatment group was injected with 74 kBq and 47 ng (21 pmol) of ^{225}Ac-RPS-074. The third treatment group was injected with 37 kBq and 23 ng (10 pmol) of ^{225}Ac-RPS-074. The fourth group was injected with the same volume of vehicle. The fifth group was injected with 133 kBq of ^{225}Ac-DOTA-Lys-IPBA. Tumor dimensions were measured and recorded 3 times weekly with digital calipers, and tumor volumes were calculated using the following modified ellipsoid equation: volume = 0.5 × length × width × width (*20*). Mice were sacrificed after tumors reached 1,500 mm^3 or if the mice showed any visible signs of distress, including loss of body weight, lack of appetite, excessive lethargy, or formation of sores and rashes. Body weight was measured with a digital balance twice weekly, and the mice were monitored for signs of distress. The mice were photographed weekly to visually confirm changes in tumor volume.

Imaging of Treated Mice by Small-Animal PET/CT

^{68}Ga-PSMA-11 (also known as ^{68}Ga-HBED-CC) was prepared as previously reported (*21*). Eight mice were injected intravenously with 5.5 MBq of ^{68}Ga-PSMA-11 at 75 d after injection of either 148 or 74 kBq of ^{225}Ac-RPS-074. The mice were imaged using small-animal PET/CT (Inveon; Siemens Medical Solutions, Inc.) at 1 h after injection after inhalation anesthetization with isoflurane. The total acquisition time was 30 min. A CT scan was obtained immediately before the acquisition for both anatomic coregistration and attenuation correction. Images were reconstructed using the Inveon software supplied by the vendor.

Dosimetry Estimation

The estimated dosimetry in humans was calculated using the biodistribution data from the mouse assuming a linear interpolation between the time points of 4 h, 24 h, 7 d, 14 d, and 21 d. The average %ID/organ was calculated using the average of the activity and organ weights of the mice at that time point. Intermediate time points at every 2 h were generated using the linear approximation, and time points were corrected for decay during the time interval between points. The residence times were calculated out to 1,000 h. The biologic half-life was determined using the sum of the %ID/organ over the 21 d of the experiment. At points beyond 504 h (21 d), the assumption was made that the radiotracer concentration in the organ did not change and that the only change was due to radioactive decay. These curves were integrated using a trapezoidal approximation, and the sum was used to determine the residence time. The estimated dose to the organ was calculated using the OLINDA/EXM program for the adult male using the appropriate radioisotope and assuming a radiobiologic effectiveness of 5 for α-particle decay.

Statistical Analysis

Statistical analysis of data was performed using Prism 6 software (GraphPad Software Inc.). Data are displayed as means with their SEMs. The *P* values for comparisons between biodistribution time points and changes in tumor volume during the therapy study were determined by an unpaired, 2-tailed *t* test using GraphPad Prism. *P* values of less than 0.05 were considered to be statistically significant. A log-rank test (Mantel–Haenszel test) was performed to compare survival outcomes using manual calculation according to published methods (*22*).

RESULTS

Chemistry and Radiochemistry

RPS-074 was synthesized in 10 steps from N^{ε}-Z-Lys-O*t*Bu.HCl, macropa-isothiocyanate, and di-*tert*-butyl (((*S*)-1-(*tert*-butoxy)-6-(3-(3-ethynylphenyl)ureido)-1-oxohexan-2-yl)carbamoyl)-L-glutamate (Supplemental Fig. 1). ^{225}Ac-RPS-074 was prepared nearly quantitatively at 25°C (Supplemental Fig. 2). When the TLC plate was visualized 1 h after being run in the mobile phase, radiochemical purity appeared to be only 85.8% (Supplemental Fig. 2) because of the presence of unbound daughter nuclei arising from decay of ^{225}Ac. However, when the TLC plate was reanalyzed 7 h later, when radiochemical equilibrium had been established, purity was confirmed to be greater than 98%. During purification and reformulation of the final product by solid-phase extraction, elution from the Sep-Pak C18 Light cartridge was inefficient. Complete elution was accomplished with neat acetic acid, but the need to buffer the eluate before injection and the fact that only small activities of ^{225}Ac-RPS-074 were required for injection led us to prefer EtOH/saline as a solvent. In contrast, DOTA-containing ^{225}Ac-RPS-072 was labeled in 49% radiochemical yield (Supplemental Fig. 2), and 75% of the activity trapped on the Sep-Pak C18 Light cartridge was successfully eluted. The lane on the TLC plate corresponding to the unpurified ^{225}Ac-RPS-072 showed a spot corresponding to free ^{225}Ac even 7 h after reanalysis. ^{225}Ac-DOTA-Lys-IPBA was synthesized in 42% radiochemical yield at 95°C, with elution from the Sep-Pak C18 Light cartridge greater than 90%. Radiochemical purity of both preparations was greater than 96%.

In Vitro Evaluation

The IC_{50} of RPS-074 was determined to be 12.0 ± 3.4 nM, a value consistent with the reported PSMA affinities of structurally analogous trifunctional ligands such as RPS-072 (*16*).

Biodistribution in LNCaP Xenograft Mice

Uptake of ^{225}Ac-RPS-074 at 4 h after injection was greatest in blood (12.3 ± 0.5 %ID/g), lungs (5.0 ± 0.2 %ID/g), kidneys (6.7 ± 0.4 %ID/g), and tumor (5.8 ± 0.3 %ID/g) (Fig. 1). By 24 h after injection, the activity in nontarget tissue, including kidneys (2.9 ± 0.3 %ID/g), cleared significantly ($P < 0.001$) in concert with blood clearance, whereas tumor activity more than doubled, reaching 12.7 ± 1.5 %ID/g. By 7 d after injection, activity in tumors remained high (9.5 ± 1.5 %ID/g), whereas the activity in blood and all other tissue decreased to less than 1 %ID/g. No significant clearance ($P = 0.72$) from tumors (11.9 ± 1.5 %ID/g) was evident

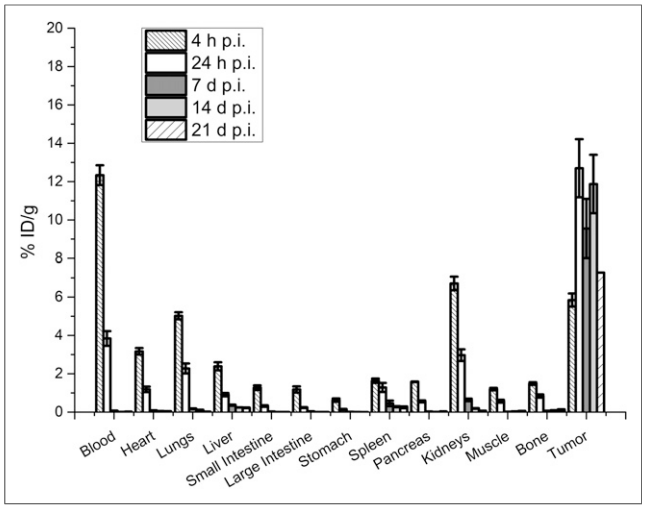

FIGURE 1. Uptake of activity in blood, normal tissue, and tumor in male BALB/C *nu/nu* mice bearing LNCaP xenograft tumors. Mice (n = 4/time point) were injected intravenously with 105 kBq of ^{225}Ac-RPS-074 and sacrificed at 4 h, 24 h, 7 d, 14 d, and 21 d after injection (p.i.).

at 14 d after injection, whereas activity in all other tissues was largely indistinguishable from background. By 21 d after injection, an antitumor was evident, with only 1 mouse still bearing a tumor, and activity in the nontarget tissue remained indistinguishable from background.

The tumor-to-kidney and tumor-to-blood ratios favored the tumor at early time points. By 24 h after injection, the tumor-to-kidney ratio reached 4.3 ± 0.7, whereas at 7 d and 14 d after injection it was 15.0 ± 2.9 and 62.2 ± 9.5, respectively. The tumor-to-blood ratio at the same time points was 3.3 ± 0.5, 137.5 ± 30.4, and 995.8 ± 139.7. Time–activity curves were plotted, and the tumor dose integral was estimated to be 3,223 %ID/g·h. In contrast, the dose integral in kidneys was 244 %ID/g·h, leading to a tumor-to-kidney ratio of 13.

The distribution of ^{225}Ac-RPS-072 at 24 h after injection was most evident in the tumor (15.9 ± 4.3 %ID/g), kidneys (5.2 ± 0.7 %ID/g), and blood (2.5 ± 0.2 %ID/g), with PSMA organs such as spleen and highly vascularized organs such as lungs and liver also showing nominal uptake (Supplemental Fig. 3). In comparison to ^{225}Ac-RPS-074 at the same time point, uptake in the kidneys was significantly higher (P = 0.024) and blood activity was significantly lower (P = 0.026). Uptake of the 2 ligands in tumors was not significantly different (P = 0.51).

Dosimetry Estimations

Whole-organ dosimetry was estimated for a human on the basis of the biodistribution of ^{225}Ac-RPS-074 in mice (Fig. 1) using OLINDA/EXM software and assuming a radiobiologic effectiveness of 5 for α-particles emitted by ^{225}Ac. The biologic half-life was 99 h, and therefore the dose estimates were made only for 1,000 h (10 biologic half-lives). Estimated dose to the tumor (440 mSv/MBq) was more than 5 times greater than total dose to the organ with the next highest dose, which was the kidney (84 mSv/MBq). The next highest organ was the heart wall, which was 40 mSv/MBq. The heart dose was due to the increased retention in the blood at early times. The full table of organs can be found in Supplemental Table 1.

Therapy Studies in LNCaP Xenograft Mice

A significant antitumor effect ($P < 0.001$) was observed in the mice treated with 148 and 74 kBq of ^{225}Ac-RPS-074 (Figs. 2A and 2B). In the 148-kBq treatment group, 6 of 7 (86%) tumors were not detectable (<0.5 mm^3) at 75 d after injection, whereas 1 of 7 (14%) tumors were not detectable in the 74-kBq group. The distribution of initial tumor volumes was 100–808 and 64–455 mm^3 for the 2 groups, respectively. Tumor volume decreased to below 1 mm^3 in 86% of mice in the 74-kBq group for as many as 42 d after injection before 6 of 7 (86%) tumor volumes began to increase again (Fig. 2B). The absence of tumors was confirmed by small-animal PET/CT imaging with ^{68}Ga-PSMA-11 (Supplemental Fig. 4) at the end of the study. Those tumors that reemerged in the 74-kBq treatment group were shown by imaging to express PSMA (Supplemental Fig. 4). Physiologic uptake was also evident in the kidneys and salivary glands.

Both the 37-kBq treatment group and the positive control group, which received 133 kBq of ^{225}Ac-DOTA-Lys-IPBA, showed an initial effect relative to the untreated group, but tumor volumes increased from a starting volume of 99–331 and 233–859 mm^3, respectively, to a final volume of greater than 1,500 mm^3 (Figs. 2C and 2D). The antitumor effect was not statistically significant for the 37-kBq group ($P > 0.20$) and was significant only up to 14 d ($P < 0.01$) for the ^{225}Ac-DOTA-Lys-IPBA group. The tumor volumes of the untreated group rapidly increased (Fig. 2E). A plot of the average change in tumor volume in each group is shown in Supplemental Figure 5.

Every mouse in the 148-kBq treatment group survived the 75-d study (Fig. 3). In contrast, in each of the other groups at least 2 mice were sacrificed before the termination of the study because of excessive tumor growth. The survival curves for the 74- and 148-kBq treatment groups were significantly different from the 37-kBq group and the 2 control groups ($P < 0.02$). The survival curves for the 37-kBq group and the 133-kBq ^{225}Ac-DOTA-Lys-IPBA positive control group were not significantly different from each other ($P > 0.10$), although the median survival time of the 37-kBq group was 33 d and the median survival time of the ^{225}Ac-DOTA-Lys-IPBA group was 42 d. Both curves were significantly different ($P < 0.02$) from the untreated group, for which the median survival time was 14 d and all animals were sacrificed by 30 d. One mouse treated with ^{225}Ac-DOTA-Lys-IPBA survived until tumor measurements were discontinued at 63 d, but the tumor volume at that time point was more than 1,300 mm^3 and rapidly increasing (Fig. 2). No overt toxic effects were visible in any of the groups. The variation in body weight during the 75-d study ranged from 92% to 106% of the original measurement (Supplemental Fig. 6).

DISCUSSION

The introduction of targeted α-therapy in humans using small-molecule inhibitors of PSMA for the treatment of mCRCP by the Heidelberg group has revealed both the great potential for tumor control and the powerful adverse effects α-particles can have on normal tissues (*11*). With this in mind, we have focused our efforts on maximizing the therapeutic window of these powerful radiopharmaceuticals. Our choice of RPS-074 for preclinical therapy studies follows the identification of the recently reported analog RPS-072 (*16*), which showed dramatically reduced kidney uptake and substantially increased and prolonged tumor uptake relative to several novel PSMA-targeting ligands, including PSMA-617,

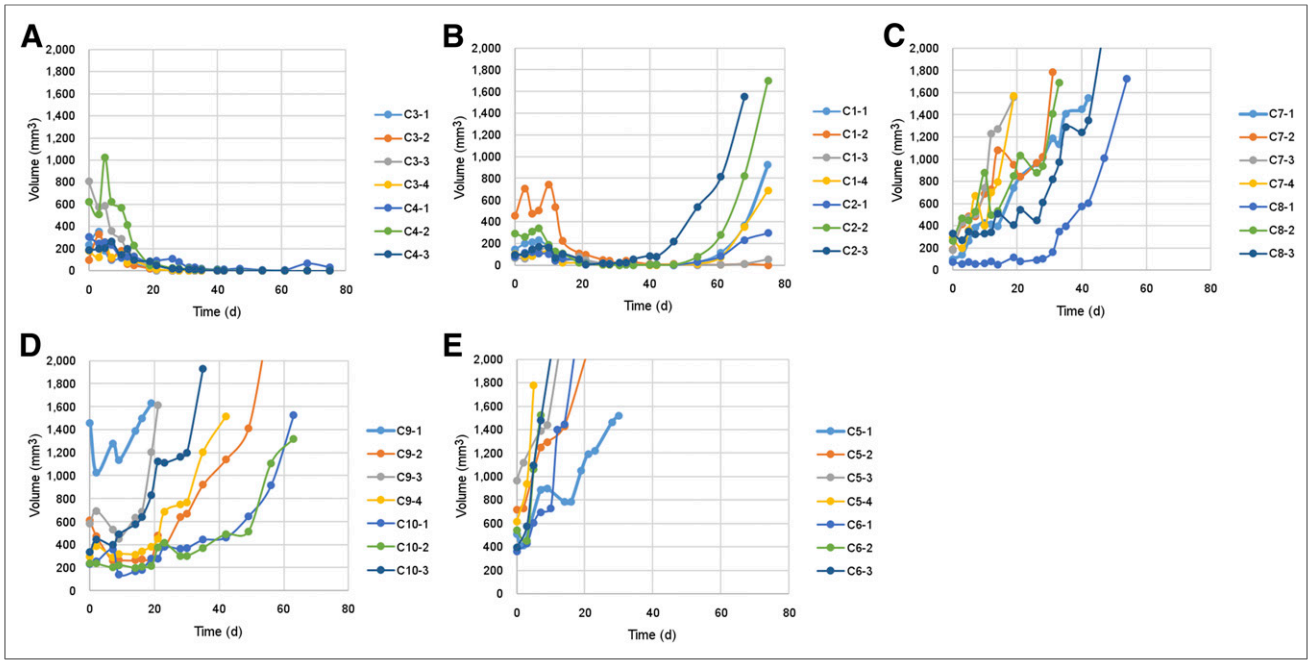

FIGURE 2. Plot of tumor volumes of individual male BALB/C *nu/nu* mice bearing LNCaP xenograft tumors and treated with 148 kBq of ^{225}Ac-RPS-074 (A), 74 kBq of ^{225}Ac-RPS-074 (B), 37 kBq of ^{225}Ac-RPS-074 (C), 133 kBq of ^{225}Ac-DOTA-Lys-IPBA (D), and vehicle (E). Mice were sacrificed when tumor volume exceeded 1,500 mm^3.

RPS-063 (*23*), CTT1403 (*24*), PSMA-Alb-02 (*19*), and PSMA-Alb-56 (*25*). Although the DOTA-containing RPS-072 also chelates $^{225}Ac^{3+}$, radiolabeling yield was only 49%, and the ^{225}Ac-DOTA complex has been found to have suboptimal in vivo stability (*26,27*). Therefore, the DOTA moiety of RPS-072 was replaced by macropa, an 18-membered macrocycle that has showed quantitative chelation of $^{225}Ac^{3+}$ at room temperature and excellent in vivo stability when conjugated to antibodies or small molecules (*15*). Chelation of $^{225}Ac^{3+}$ by RPS-074 was quantitative, potentially eliminating the need for subsequent purification. Typically, radio-TLC has been the preferred method of determining radiochemical purity, but it is necessary to delay the visualization of the TLC strip from 1 h (*11*) to up to 24 h (*28*) until the radiochemical equilibrium between ^{225}Ac and its daughter nuclides is reached. We found that a measurement time of 8 h gave a more accurate representation of radiochemical purity than 1 h (Supplemental Fig. 2) and could successfully distinguish between free ^{225}Ac and its unbound daughter nuclides. Therefore, we decided to preemptively perform purification by solid-phase extraction to ensure that the radioligand could be administered to the mice on the same day of its preparation and consequently minimize the risk of radiolysis. Work to establish the minimum delay in TLC analysis that predicts radiochemical purity with sufficient accuracy is ongoing.

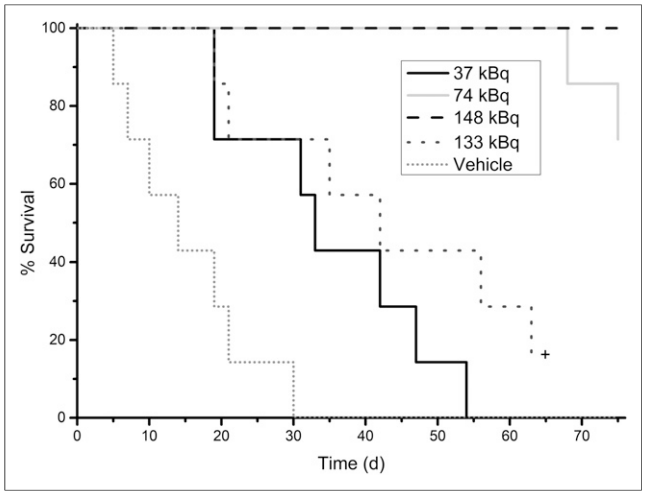

FIGURE 3. Kaplan–Meier plot comparing survival of male BALB/c *nu/nu* mice (n = 7/group) bearing LNCaP xenograft tumors treated with 37, 74, or 148 kBq of ^{225}Ac-RPS-074; 133 kBq of ^{225}Ac-DOTA-Lys-IPBA; or vehicle. Mice were sacrificed when tumor volume exceeded 1,500 mm^3. + = censored mouse that was removed from study before endpoint at 75 d.

In comparison to the biodistribution of ^{177}Lu-RPS-072 at 96 h (*16*), the distribution kinetics were nearly identical, although ^{225}Ac-RPS-074 showed slightly lower tumor uptake and more rapid clearance from blood than its DOTA-based counterpart at 24 h. It appears that the choice of radionuclide is predominantly responsible for the decreased tumor uptake, because uptake of ^{225}Ac-RPS-072 at 24 h after injection (Supplemental Fig. 3) was more similar to ^{225}Ac-RPS-074 than that reported for ^{177}Lu-RPS-072 (34.9 ± 2.4 %ID/g) at the same time point. The similar in vivo behavior of ^{225}Ac-RPS-074 and ^{225}Ac-RPS-072 should enable RPS-072 radiolabeled with ^{111}In to serve as a surrogate for RPS-074 in the calculation of dosimetry and the selection of initial therapy doses, thus facilitating rapid clinical translation.

As our experiences with the macropa chelator would predict, ^{225}Ac-RPS-074 showed excellent in vivo stability over 3 wk in vivo. No accumulation of signal was evident in the liver or bone, 2 organs in which free $^{225}Ac^{3+}$ typically accumulates (*29*). Initial uptake in organs such as the lungs corresponds to their degree of vascularization, suggesting that the signal reflects blood pooling

rather than uptake. This suggestion is confirmed by the clearance profile from normal tissue, which coincides with clearance of activity from blood.

In comparison to ^{225}Ac-PSMA-617, our data suggest that ^{225}Ac-RPS-074 exhibits an improved therapeutic index. The mean absorbed dose in kidneys is 10-fold lower than calculated for ^{225}Ac-PSMA-617 in human patients (*30*). In turn, the kidney dose is more than 1,000-fold lower than that of ^{211}At-6, a small-molecule PSMA inhibitor (*31*), for which 37 kBq was the maximum tolerated dose because of late radiation necropathy. Despite the decreased rate of clearance from blood of ^{225}Ac-RPS-074 relative to ^{225}Ac-PSMA-617, the dose to the heart wall increased by a factor of only 2. These findings support the approach of using enhanced albumin binding as a method of increasing therapeutic index.

A clear dose response was evident in the current therapy study. On the basis of the average change in tumor volume (Supplemental Fig. 5), both of the higher-dose treatment groups were significantly different ($P < 0.002$) from the untreated group by 7 d after injection. The tumors of the mice in the 37-kBq treatment group appeared to grow at a similar rate to the untreated tumors, although a clear survival benefit was observed. The ^{225}Ac-DOTA-Lys-IPBA treatment group controlled for the antitumor effect of circulating ^{225}Ac, as the Lys-IPBA moiety has been shown to bind serum albumin with high affinity (*32*) and LNCaP tumors are reported to be well vascularized (*33*). Although comparison to the untreated group suggests that there is a small antitumor effect caused by 133 kBq of ^{225}Ac with a long circulation half-life, this effect is neither prolonged relative to the 74- and 148-kBq groups ($P \leq 0.05$ at 14 d) nor significant relative to the vehicle group ($P = 0.22$) by 21 d.

The range of initial tumor volumes was very large even though the mice were inoculated at the same time. Moreover, palpable tumors emerged in the mice in 2 distinct phases. Those that emerged approximately 8 wk after inoculation, which included 3 of 7 of the vehicle group and 7 of 7 of the ^{225}Ac-DOTA-Lys-IPBA group, developed more slowly than those tumors that emerged approximately 6 wk after inoculation. It is likely that the slower growth of this second group of tumors contributed to any apparent survival benefit conferred by ^{225}Ac-DOTA-Lys-IPBA: the survival curves of this group and the second vehicle group ($n = 3$) were not significantly different ($P > 0.05$).

The uneven growth of LNCaP tumors represents a challenge to using this xenograft tumor model relative to cell lines such as PC3-PIP. However, PSMA expression levels in PC3-PIP cells are increased by 10-fold relative to expression levels in LNCaP cells (*31*). Consequently, uptake of PSMA-targeting ligands in PC3-PIP tumors might be unrealistically high and the corresponding biodistribution and therapy studies potentially misleading. Therefore, we chose the LNCaP model despite the heterogeneous distribution of tumor growth rates. It seems likely that at least 1 of the mice of the untreated group and 2 of the mice of the DOTA-Lys-IPBA group experienced unusually slow tumor growth as a result of the biologic heterogeneity of the LNCaP model.

In this light, the response to 148 kBq of ^{225}Ac-RPS-074 is even more encouraging, as tumors as large as 624–808 mm^3 showed a complete response. To our knowledge, few accounts of preclinical therapy studies of PSMA-targeting α-radioligand therapeutics have been reported, and none have shown such a profound antitumor effect. ^{213}Bi-PSMA-I&T was shown to induce double-strand breaks in LNCaP xenograft tumor cells, but tumor uptake was low (5.75 ± 2.70 %ID/g at 1 h after injection), tumor-to-kidney ratio poor (0.19 ± 0.10), and relatively few α-tracks and double-strand breaks were evident in the tumor 24 h after injection (*34*). An investigation of ^{211}At-6 was conducted in mice bearing subcutaneous PC3-PIP tumors with a maximum initial volume of 200 mm^3 (*31*). Although a small antitumor effect was observed after a single injection of 740 kBq of ^{211}At-6, the maximum tolerated dose was just 37 kBq.

CONCLUSION

^{225}Ac-RPS-074 demonstrates high and prolonged accumulation in LNCaP xenograft tumors, with uptake being a function of both its high affinity for PSMA and its favorable pharmacokinetics resulting from an extended blood clearance profile. Mice treated with a single dose of 74 kBq of ^{225}Ac-RPS-074 showed a dramatic, albeit ultimately reversible, antitumor effect, whereas mice treated with a single dose of 148 kBq of ^{225}Ac-RPS-074 exhibited complete tumor remission by approximately 21 d after injection, with the absence of tumors confirmed by both small-animal PET/CT imaging and dissection. The high tumor uptake and clear antitumor effect, combined with the broad therapeutic index, of ^{225}Ac-RPS-074 make it a ligand with significant potential for treatment of prostate cancer by PSMA-targeted α-radiotherapy and a leading candidate for clinical translation.

DISCLOSURE

James M. Kelly, Alejandro Amor-Coarasa, Shashikanth Ponnala, Nikki A. Thiele, Justin J. Wilson, and John W. Babich hold intellectual property rights on compounds described in this work. James M. Kelly, Alejandro Amor-Coarasa, Shashikanth Ponnala, Justin J. Wilson, and John W. Babich hold equity in Noria Therapeutics, Inc. No other potential conflict of interest relevant to this article was reported.

ACKNOWLEDGMENTS

We acknowledge Dr. J. David Warren for access to services in the Milstein Chemistry Core Facility at Weill Cornell Medicine, Prof. Shankar Vallabhajosula for his advice on the handling and disposal of ^{225}Ac, and Julie Urgiles for her assistance with tumor measurements.

REFERENCES

1. Nussbaum N, George DJ, Abernethy AP, et al. Patient experience in the treatment of metastatic castration-resistant prostate cancer: state of the science. *Prostate Cancer Prostatic Dis.* 2016;19:111–121.
2. Rahbar K, Schmidt M, Heinzel A, et al. Response and tolerability of a single dose of ^{177}Lu-PSMA-617 in patients with metastatic castration-resistant prostate cancer: a multicenter retrospective analysis. *J Nucl Med.* 2016;57:1334–1338.
3. Rahbar K, Ahmadzadehfar H, Kratochwil C, et al. German multicenter study investigating ^{177}Lu-PSMA-617 radioligand therapy in advanced prostate cancer patients. *J Nucl Med.* 2017;58:85–90.
4. Rahbar K, Boegemann M, Yordanova A, et al. PSMA targeted radioligand therapy in metastatic castration resistant prostate cancer after chemotherapy, abiraterone and/or enzalutamide: a retrospective analysis of overall survival. *Eur J Nucl Med Mol Imaging.* 2018;45:12–19.
5. Hoffman MS, Violet J, Hicks RJ, et al. [^{177}Lu]-PSMA-617 radionuclide treatment in patients with metastatic castration-resistant prostate cancer (LuPSMA trial): a single-centre, single-arm, phase 2 study. *Lancet Oncol.* 2018;19:825–833.
6. Kim YJ, Kim YI. Therapeutic responses and survival effects of ^{177}Lu-PSMA-617 radioligand therapy in metastatic castrate-resistant prostate cancer: a meta-analysis. *Clin Nucl Med.* 2018;43:728–734.

7. Baum RP, Kulkarni HR, Schuchardt C, et al. Lutetium-177 PSMA radioligand therapy of metastatic castration-resistant prostate cancer: safety and efficacy. *J Nucl Med.* 2016;57:1006–1013.
8. Heck MM, Retz M, D'Alessandria C, et al. Systemic radioligand therapy with ^{177}Lu labeled prostate specific membrane antigen ligand for imaging and therapy in patients with metastatic castration resistant prostate cancer. *J Urol.* 2016;196:382–391.
9. Zechmann CM, Afshar-Oromieh A, Armor T, et al. Radiation dosimetry and first therapy results with a ^{124}I/^{131}I-labeled small molecule (MIP-1095) targeting PSMA for prostate cancer therapy. *Eur J Nucl Med Mol Imaging.* 2014;41: 1280–1292.
10. Afshar-Oromieh A, Haberkorn U, Zechmann C, et al. Repeated PSMA-targeting radioligand therapy of metastatic prostate cancer with ^{131}I-MIP-1095. *Eur J Nucl Med Mol Imaging.* 2017;44:950–959.
11. Kratochwil C, Bruchertseifer F, Giesel FL, et al. ^{225}Ac-PSMA-617 for PSMA-targeted α-radiation therapy of metastatic castration-resistant prostate cancer. *J Nucl Med.* 2016;57:1941–1944.
12. Denis-Bacelar AM, Chittenden SJ, Murray I, et al. A radiobiological model of metastatic burden reduction for molecular radiotherapy: application to patients with bone metastases. *Phys Med Biol.* 2017;62:2859–2870.
13. Langbein T, Chaussé G, Baum RP. Salivary gland toxicity of PSMA radioligand therapy: relevance and preventative strategies. *J Nucl Med.* 2018;59:1172–1173.
14. Kelly J, Amor-Coarasa A, Nikolopoulou A, et al. Synthesis and pre-clinical evaluation of a new class of high-affinity ^{18}F-labeled PSMA ligands for detection of prostate cancer by PET imaging. *Eur J Nucl Med Mol Imaging.* 2017;44:647–661.
15. Thiele NA, Brown V, Kelly JM, et al. An eighteen-membered macrocyclic ligand for actinium-225 targeted alpha therapy. *Angew Chem Int Ed Engl.* 2017;56:14712–14717.
16. Kelly JM, Amor-Coarasa A, Ponnala S, et al. Albumin-binding PSMA ligands: implications for expanding the therapeutic window. *J Nucl Med.* December 14, 2018 [Epub ahead of print].
17. Hillier SM, Maresca KP, Lu G, et al. ^{99m}Tc-labeled small-molecule inhibitors of prostate-specific membrane antigen for molecular imaging of prostate cancer. *J Nucl Med.* 2013;54:1369–1376.
18. Kelly JM, Amor-Coarasa A, Nikolopoulou A, et al. Dual-target binding ligands with modulated pharmacokinetics for endoradiotherapy of prostate cancer. *J Nucl Med.* 2017;58:1442–1449.
19. Benešová M, Umbricht CA, Schibli R, Müller C. Albumin-binding PSMA ligands: optimization of the tissue distribution profile. *Mol Pharm.* 2018;15:934–946.
20. Jensen MM, Jørgensen JT, Binderup T, Kjær A. Tumor volume in subcutaneous mouse xenografts measured by microCT is more accurate and reproducible than determined by ^{18}F-FDG-microPET or external caliper. *BMC Med Imaging.* 2008;8:16.
21. Amor-Coarasa A, Kelly JM, Gruca M, Nikolopoulou A, Vallabhajosula S, Babich JW. Continuation of comprehensive quality control of the itG ^{68}Ge/^{68}Ga generator and production of ^{68}Ga-DOTATOC and ^{68}Ga-PSMA-HBED-CC for clinical research studies. *Nucl Med Biol.* 2017;53:37–39.
22. Bewick V, Cheek L, Ball J. Statistics review 12: survival analysis. *Crit Care.* 2004;8:389–394.
23. Kelly J, Amor-Coarasa A, Ponnala S, et al. Trifunctional PSMA-targeting constructs for prostate cancer with unprecedented localization to LNCaP tumors. *Eur J Nucl Med Mol Imaging.* 2018;45:1841–1851.
24. Choy CJ, Ling X, Geruntho JJ, et al. ^{177}Lu-labeled phosphoramidate-based PSMA inhibitors: the effect of an albumin binder on biodistribution and therapeutic efficacy in prostate tumor-bearing mice. *Theranostics.* 2017;7:1928–1939.
25. Umbricht CA, Benešová M, Schibli R, Müller C. Preclinical development of novel PSMA-targeting radioligands: modulation of albumin-binding properties to improve prostate cancer therapy. *Mol Pharm.* 2018;15:2297–2306.
26. Deal KA, Davis IA, Mirzadeh S, Kennel SJ, Brechbiel MW. Improved in vivo stability of actinium-225 macrocyclic complexes. *J Med Chem.* 1999;42: 2988–2992.
27. Fitzsimmons J, Nayak T, Cutler C, Atcher R. Synthesis and preliminary biological evaluations of fluorescent of ^{149}promethium labeled trastuzumab-polyethylenimine. *Biomedicines.* 2016;4:E1.
28. Pandya DN, Hantgan R, Budzevich MM, et al. Preliminary therapy evaluation of ^{225}Ac-DOTA-c (RGDyK) demonstrates that Cerenkov radiation derived from ^{225}Ac daughter decay can be detected by optical imaging for in vivo tumor visualization. *Theranostics.* 2016;6:698–709.
29. Miederer M, Scheinberg DA, McDevitt MR. Realizing the potential of the actinium-225 radionuclide generator in targeted alpha-particle therapy applications. *Adv Drug Deliv Rev.* 2008;60:1371–1382.
30. Kratochwil C, Bruchertseifer F, Rathke H, et al. Targeted α-therapy of metastatic castration-resistant prostate cancer with ^{225}Ac-PSMA-617: dosimetry estimate and empiric dose finding. *J Nucl Med.* 2017;58:1624–1631.
31. Kiess AP, Minn I, Vaidyanathan G, et al. (2S)-2-(3-(1-Carboxy-5-(4-^{211}At-astatobenzamido)pentyl)ureido)-pentanedioic acid for PSMA-targeted α-particle radiopharmaceutical therapy. *J Nucl Med.* 2016;57:1569–1575.
32. Dumelin CE, Trüssel S, Buller F, et al. A portable albumin binder from a DNA-encoded chemical library. *Angew Chem Int Ed Engl.* 2008;47:3196–3201.
33. Byrne NM, Nesbitt H, Ming L, McKeown SR, Worthington J, McKenna DJ. Androgen deprivation in LNCaP prostate tumour xenografts induces vascular changes and hypoxic stress, resulting in promotion of epithelial-to-mesenchymal transition. *Br J Cancer.* 2016;114:659–668.
34. Nonnekens J, Chatalic KLS, Molkenboer-Kuenen JDM, et al. ^{213}Bi-labeled prostate-specific membrane antigen-targeting agents induce DNA double-strand breaks in prostate cancer xenografts. *Cancer Biother Radiopharm.* 2017;32: 67–73.